1 **Modeling biogenic secondary organic aerosol (BSOA) formation from monoterpene**
2 **reactions with NO₃: A case study of the SOAS campaign using CMAQ**

3 Momei Qin[a,e], Yongtao Hu[b], Xuesong Wang[a,*], Petros Vasilakos[c], Christopher M. Boyd[c], Lu
4 Xu[c,h], Yu Song[a], Nga Lee Ng[c,d], Athanasios Nenes[c,d, i, j], Armistead G. Russell[b,*]

5 a State Key Joint Laboratory of Environmental Simulation and Pollution Control, College of
6 Environmental Sciences and Engineering, Peking University, Beijing, China.
7 b School of Civil and Environmental Engineering, Georgia Institute of Technology, Atlanta, GA,
8 USA.
9 c School of Chemical & Biomolecular Engineering, Georgia Institute of Technology, Atlanta,
10 GA, USA.
11 d School of Earth and Atmospheric Sciences, Georgia Institute of Technology, Atlanta, GA,
12 USA.
13 e Now at School of Civil and Environmental Engineering, Georgia Institute of Technology,
14 Atlanta, GA, USA.
15 h Now at Division of Geological and Planetary Sciences, California Institute of Technology,
16 Pasadena, CA, USA.
17 i Institute of Chemical Engineering Sciences, Foundation for Research and Technology-Hellas,
18 Patras, Greece
19 j Institute for Environmental Research and Sustainable Development, National Observatory of
20 Athens, Palea Penteli, Greece

21

22 **Abstract**

23 Monoterpenes react with nitrate radicals (NO₃), contributing substantially to nighttime organic
24 aerosol (OA) production. In this study, the role of reactions of monoterpenes + NO₃ in forming
25 biogenic secondary organic aerosol (BSOA) was examined using the Community Multiscale Air
26 Quality (CMAQ) model, with extended emission profiles of biogenic volatile organic
27 compounds (BVOCs), species-specific representations of BSOA production from individual
28 monoterpenes and updated aerosol yields for monoterpene + NO₃. The model results were
29 compared to detailed measurements from the Southern Oxidants and Aerosol Study (SOAS) at
30 Centreville, Alabama. With the more detailed model, monoterpene-derived BSOA increased by
31 ~1 μg·m⁻³ at night, accounting for one-third of observed less-oxidized oxygenated OA
32 (LO-OOA), more closely agreeing with observations (lower error, stronger correlation).
33 Implementation of a multigenerational oxidation approach resulted in the model capturing
34 elevated OA episodes. With the aging model, aged semi-volatile organic compounds (ASVOCs)
35 contributed over 60% of the monoterpene-derived BSOA, followed by SOA formation via nitrate
36 radical chemistry, making up to 34% of that formed at night. Among individual monoterpenes,
37 β-pinene and limonene contributed most to the monoterpene-derived BSOA from nighttime
38 reactions.

39 **Key words**: Biogenic aerosol, Secondary Organic Aerosol, BSOA, monoterpene, CMAQ,
40 multigenerational oxidation, SOAS

1. Introduction

Biogenic secondary organic aerosol (BSOA), formed from biogenic volatile organic compounds (BVOCs), impacts air quality and global climate (Geddes et al., 2016; Heald and Geddes, 2016; Zhang and Wang, 2016). Isoprene (C_5H_8), the most abundant non-methane volatile organic compound (VOC), monoterpenes (isomers of $C_{10}H_{16}$), and sesquiterpenes ($C_{15}H_{24}$), are estimated to contribute ~30% of organic aerosol (OA) annually on a global scale (Pye et al., 2010). In the summertime, particularly in the southeastern United States (SE US), biogenic emissions play an even more important role, being responsible for over half of observed OA (Kleindienst et al., 2007; Offenberg et al., 2011; Weber et al., 2007; Xu et al., 2015a).

Production of isoprene-formed BSOA (hereafter as SOA_I), initialized by photo-oxidation of isoprene with aqueous uptake of isoprene epoxydiols (IEPOX) and subsequent addition of nucleophiles (*e.g.* H_2O, inorganic sulfate), has been extensively investigated (Kroll et al., 2006; Kroll and Seinfeld, 2008; Kuwata et al., 2015; Lin et al., 2013; Liu et al., 2015; Nguyen et al., 2014b; Rollins et al., 2012; Surratt et al., 2010; Surratt et al., 2007; Surratt et al., 2006; Vasilakos, 2018; Worton et al., 2013; Xu et al., 2015a; Xu et al., 2014). Its mechanism has already been implemented into chemistry transport models such as the Community Multiscale Air Quality (CMAQ) and GEOS-Chem (Byun and Schere, 2006; Jathar et al., 2016; Pye et al., 2013; Xie et al., 2013). Parameterization of SOA_I formation in CMAQ was further revised to reflect the fact that SOA_I is primarily mediated by the abundance of sulfate instead of the particle water content and/or particle acidity as suggested by prior laboratory studies (Vasilakos, 2018; Xu et al., 2015a). Xu et al. (2015a) also reported that monoterpenes reacting with nitrate radical (NO_3) account for ~50% of the night time OA production at Centreville, Alabama, and this large contribution is likely due to high levels of monoterpenes at night and their high SOA yields. Elevated levels of nighttime organonitrates were also observed in the southeastern US (Xu et al., 2015b), California (Rollins et al., 2012), and at multiple sites worldwide (Ng et al., 2017), particularly in areas influenced by both biogenic and anthropogenic emissions.

NO_3, which is expected to be an essential precursor to nighttime BSOA formation, is mainly produced via the reaction between O_3 (ozone) and NO_2 (nitrogen dioxide). Daytime concentrations of NO_3 are low due to rapid photolysis and reaction with NO but can still reach a few hundred ppt in urban plumes at night (Penkett et al., 2007; Seinfeld and Pandis, 2012). It can oxidize monoterpenes by attacking the double bonds to form organonitrates ($RONO_2$). Fry et al. (2014) pointed out that chamber study-determined aerosol yields of monoterpene + NO_3 vary dramatically among different monoterpenes, ranging from zero for α-pinene (one of the most abundant individual monoterpenes) to 44% for limonene at a mass loading of 10 $\mu g \cdot m^{-3}$. A substantial fraction (56-82%) of the aerosol is organonitrate. As summarized in Table 2 in Ng et al. (2017), little aerosol production (yield <16% at mass loading up to a few hundred $\mu g \cdot m^{-3}$) for NO_3 oxidation of α-pinene was also reported from other chamber studies (Hallquist et al., 1999; Moldanova and Ljungström, 2000; Nah et al., 2015; Perraud et al., 2010; Spittler et al., 2006). SOA yields for β-pinene + NO_3 are higher, varying up to 104% for a broad range of mass loading (5.1-216.1 $\mu g \cdot m^{-3}$) (Boyd et al., 2015). Reactions of limonene with NO_3 produce BSOA more efficiently, with approximately a constant yield of 174% at 298K, independent of organic mass loadings (Boyd et al., 2017). This is higher than a previously reported range of 20% (Hallquist et

83   al., 1999) to ~40% (Fry et al., 2011; Fry et al., 2009), potentially because it was obtained under

84   conditions that both of the double bonds were oxidized mainly by NO_3.

85   Even though current SOA yields are determined by environmental chamber studies at

86   atmospherically-relevant concentrations, chemical transport models have difficulty reproducing

87   observed OA in the atmosphere with the yields on the magnitude and on the properties, e.g.

88   oxidation state, indicated by atomic oxygen-to-carbon (O:C) ratios (Chen et al., 2015; Hallquist

89   et al., 2009; Hayes et al., 2015; Li et al., 2015; Yu et al., 2007). For example, a review reported

90   that nearly half of the 10 targeted studies had modeled OA ~50% lower than the reported

91   measured values coming from the existing networks such as the Chemical Speciation Network

92   (CSN) and the Interagency Monitoring of Protected Visual Environments network (IMPROVE)

93   in the U.S.(Simon et al., 2012). Losses of semi-volatile organic compounds (SVOCs), or

94   particles to chamber walls, which were an issue while are currently being reduced, could lead to

95   lower yields than in the atmosphere, and in part explain the model-measurement discrepancies

96   (La et al., 2016; Nah et al., 2017; Nah et al., 2016; Nah et al., 2015; Zhang et al., 2014).

97   More likely, further reactions of intermediate products, e.g. multigenerational oxidation of

98   SVOCs, either in the gaseous phase or the condensed phase, were not well captured in the

99   chamber. With multigenerational oxidation, the products partitioned appreciably to the

100   condensed phase as a result of decreased volatility and an increased oxidation state (Donahue et

101   al., 2011; Donahue et al., 2012b; Koo et al., 2014). Experiments studying limonene (which has

102   two double bonds) and β-pinene with NO_3 indicate further oxidation and SOA growth observed

103   for limonene but not for β-pinene (Fry et al., 2011; Fry et al., 2009); Boyd et al. (2015) observed

104   a small increase in O:C for β-pinene under NO_3 aging. During photochemical aging, α-pinene

105   and β-pinene BSOA initially via NO_3 chemistry becomes increasingly oxidized (Nah et al., 2015).

106   On the other hand, Aumont et al. (2012) estimated that the timescale required to reach the

107   maximum yield resulting from successive oxidation steps in the atmosphere exceeds one week

108   for decane which may increase as organic aerosol loading or hydrocarbon carbon chain length

109   decreases. With the same number of carbon atoms, monoterpene-formed BSOA (hereafter as

110   SOA_M) likely increases to a maximum in multiple days, longer than chamber experiment

111   duration. Although aging of α-pinene formed BSOA via NO_3 chemistry could be an exception

112   since the BSOA re-volatilize and partition back to the gas phase (Nah et al., 2015).

113   Multigenerational oxidation occurring in a biogenic environment can alter the amount of SOA

114   beyond that observed in chambers (Palm et al., 2016).

115   Monoterpene BSOA production via NO_3 chemistry is frequently parameterized using the Odum

116   two-product fit (Odum et al., 1996), volatility basis set (VBS) approach (Henry and Donahue,

117   2012), or fixed yield to estimate gas/particle partitioning of semi-volatile products from initial

118   hydrocarbon reactions in atmospheric chemistry transport models (Table 5 in Ng et al. (2017)).

119   Previous modeling studies have found that NO_3 oxidation contributes 10-20% of global SOA,

120   primarily originating from terpenes, and is more important in polluted regions (Allen et al., 2015;

121   Pye et al., 2010). Yields for photo-oxidation of monoterpenes (Griffin et al., 1999) are adopted

122   for monoterpene + NO_3 parameterization in regional models, e.g. CMAQ and CAMx using the

123   two-product approach, which likely underestimates nocturnal BSOA production based on recent

124   field (Xu et al., 2015a) and experimental studies (Boyd et al., 2017; Boyd et al., 2015). A lack of

the knowledge of the reaction products, including identity and volatility, hinder specifying further reactions in monoterpene + NO$_3$ chemistry. For instance, the potentially short lifetime of particulate organonitrates (τ=2.1-4.0h) or rapid hydrolysis rate (τ=3h) is needed for optimal model-observation agreement (Lee et al., 2016; Pye et al., 2015). However, laboaotry studies suggest that organic nitrates formed from photooxidaiton vs. NO$_3$ oxidation can have drastically different hydrolysis lifetimes (Boyd et al., 2015; Rindelaub et al., 2015; Bean and Hildebrandt Ruiz, 2016; Boyd et al., 2017) which is likely due to the presence of different amounts primary/secondary/tertiary nitrates (Darer et al., 2011; Hu et al., 2011). Most organonitrates from β-pinene + NO$_3$ undergo hydrolysis at a low rate (τ=30h) as a result of the primary position of nitrate functional group (Boyd et al., 2015). As such, the fate of condensed organonitrates is still uncertain, and more laboratory work is warranted.

In this study, the role of monoterpene + NO$_3$ chemistry in BSOA formation was evaluated using CMAQ with updated yields based on chamber studies of β-pinene and limonene reactions with NO$_3$ (Boyd et al., 2017; Boyd et al., 2015). Given the significantly varied BSOA yields among monoterpenes, BSOA production from individual monoterpenes was represented. This method was used instead of utilizing the original lumping scheme in which parameters for five different monoterpenes are lumped together using U.S. emissions-based weighting factors (Carlton et al., 2010; Carter, 2010a). The influence of multigenerational oxidation with oxidants OH/O$_3$ which is often underestimated in chamber studies was also considered. The revised model is assessed using detailed measurements taken at Centreville, Alabama during the Southern Oxidant and Aerosol Study (SOAS) (http://soas2013.rutgers.edu).

2. Methods

2.1 Observations description

We utilized the observations from SOAS (Allen et al., 2015; Brophy and Farmer, 2015; Carlton et al., 2013; Nguyen et al., 2014a), a collaborative field campaign taking place during June 1 - July 15, 2013 to understand the interactions of biogenic and anthropogenic emissions in the SE US. The site, as part of Southeastern Aerosol Research and Characterization (SEARCH) network (Edgerton et al., 2005, 2006; Hansen et al., 2003), is located in the National Talladega Forest near Centreville (CTR), Alabama. Due to the intense emissions of BVOCs, e.g. isoprene, α-pinene, and β-pinene at the site, biogenic emissions were expected to contribute substantially to SOA in this region. Specific observations used here include OA, of which four subtypes were identified with positive matrix factorization (PMF) (Paatero and Tapper, 1994; Xu et al., 2015a). The four subtypes were biomass burning OA (BBOA), isoprene-derived SOA (isop_OA), less-oxidized oxygenated OA (LO-OOA), and more-oxidized oxygenated OA (MO-OOA). LO-OOA accounted for ~30% of OA at CTR and is associated with organic nitrates which are formed by reactions of monoterpenes via NO$_3$ chemistry. Additionally, observations of major gases (e.g. CO, NO$_2$, O$_3$ and gaseous organic nitrates), short-lived trace gases (e.g. OH radical and NO$_3$ radical), and aerosols (e.g. sulfate, nitrate, ammonium, EC, and OC) were used for model evaluation. Steady state NO$_3$ concentration (NO$_3$ $_{SS}$) calculated by Ayres et al. (2015) was regarded as the observation as NO$_3$ concentration was extremely low at CTR during the SOAS and below the lower detection limit most of the time.

2.2 Chemical Transport Modeling

The Community Multiscale Air Quality (CMAQ) model (v5.02) ((Byun and Schere, 2006), with additional updates on BSOA from isoprene oxidation products when mixed with anthropogenic pollutants (Pye et al., 2013; Vasilakos, 2018), was employed as the base model to simulate BSOA over the United States. Emissions were based on the 2011 National Emissions Inventory processed by the Sparse Matrix Operator Kernel for Emissions (version 3.5.1) (Houyoux and Vukovich, 1999). Meteorological fields were developed using the Weather Research and Forecasting (WRF) model (version 3.6) (Skamarock et al., 2005), as described in Hu et al. (2015). The Biogenic Emissions Inventory System Version 3 (BEIS3), which is embedded into the CMAQ, was adopted to run online for calculating biogenic emissions. The horizontal resolution for modeling was 36-km. The simulation period went from May 28 - July 15, 2013, covering the period of the SOAS campaign with a 4-day spin-up period. We conducted a reference simulation (called "base case" hereafter) and other simulations using two revised models. The first was the detailed model ("detailed case") which used an updated parameterization of SOA formed from monoterpenes and a more detailed description of monoterpene species from their emission through their oxidation. The second was the aging model ("aging case") which included multigenerational aging based on the detailed model. Specific changes made to CMAQ are detailed below. Emission profiles for monoterpene were adjusted in the detailed/aging cases to reproduce observed monoterpene concentrations at CTR.

2.2.1 Detailed terpene emissions

Monoterpene inventory in the base case included emissions of α-pinene and other monoterpenes. In the detailed case and the aging case, emissions of individual monoterpenes, e.g. α-pinene, β-pinene, limonene, Δ3-carene, and sabinene, were calculated respectively, along with aggregated emission of the remaining monoterpenes including myrcene, ocimene, camphene, etc. Detailed monoterpene emissions were examined and subsequently adjusted according to a comparison between the observed individual monoterpene mixing ratios and an additional simulation using the detailed model. However, no modification of the mass or timing of total biogenic emissions was made. Based on this investigation, diurnal emission rates of the monoterpene species with the highest emission rates (α-pinene, β-pinene, and limonene) were modified iteratively until the observed diurnal variations in the detailed/aging cases were better captured.

2.2.2. Updated parameterization of SOA_M

The base case gas-phase chemistry used in CMAQ was based on the SAPRC07tic mechanism (Xie et al., 2013), which included a more explicit description of isoprene chemistry than the earlier version SAPRC07TC (Carter, 2010a, b). In the standard SARPC07tic mechanism, monoterpenes, except α-pinene, were represented ("lumped") together as "TERP", with a lumped reaction rate coefficient derived using four primary species, including β-pinene, limonene, Δ3-carene and sabinene in the North American biogenic inventory (Carter, 2010a). In this work, the oxidation of the four monoterpenes by O_3, OH, O^3P, and NO_3, were represented explicitly with an individual reaction rate constant and products (Table S1). All other monoterpenes (e.g., myrcene, ocimene, camphene, etc.) were lumped as OTERP and were

207 represented in the same way as TERP in the standard mechanism with reaction rate constant
208 derived based on Atkinson and Arey (2003), being 1.43×10^{-10} $cm^3\cdot molec^{-1}\cdot s^{-1}$, 4.52×10^{-16}
209 $cm^3\cdot molec^{-1}\cdot s^{-1}$ and 9.2×10^{-12} $cm^3\cdot molec^{-1}\cdot s^{-1}$ for reactions with OH, O_3, and NO_3 at 298K,
210 respectively. The reaction rate constant for OTERP+O^3P remained unchanged.

211 In the aerosol module, yields (α_1, α_2) and partitioning parameters (c_1^*, c_2^*) for reactions of
212 individual monoterpenes with O_3, OH, and O^3P were based on Table S-1 of Carlton et al. (2010).
213 The yields and partitioning parameters for nitrate radical chemistry of β-pinene and limonene
214 were updated according to the measured yield curve for β-pinene + NO_3 (Table S2) and limonene
215 + NO_3, respectively (Boyd et al., 2017; Boyd et al., 2015). The estimated aerosol yield (174%)
216 for limonene+NO_3 at 298K was adopted in this work by assuming that the aerosol type was
217 non-volatile. Nocturnal SOA formation from Δ3-carene and sabinene were represented with the
218 same parameters as β-pinene due to the unavailability of parameters specific to those species. As
219 in the chamber study, only a small quantity of BSOA was formed via α-pinene + NO_3 (Fry et al.,
220 2014; Nah et al., 2015), and the yield of first-generation gas-phase products was assumed to be
221 zero.

222 2.2.3 Multigenerational oxidation

223 The multigenerational oxidation of semi-volatile organic compounds (SVOCs) from
224 anthropogenic and biogenic precursors incorporated in the aging model followed the work of Baek
225 et al. (2011). SOA$_I$ formation through key intermediates IEPOX/MAPN is fundamentally a
226 process of gas-phase multigenerational oxidation followed by reactive uptake and condensation on
227 particles (Surratt et al., 2010), which was taken into account in the base model so that no further
228 reactions were added for SOA$_I$ formation. In this study, multigenerational oxidation was described
229 in a simplified manner, considering a decrease in the volatility of products with each oxidation
230 step. Aged SVOCs (ASVOCs) contributed by monoterpene, sesquiterpene, and anthropogenic
231 VOCs emissions were derived from reactions of SVOCs with OH radical and O_3, utilizing the
232 same reaction rate coefficients as the precursors in SAPRC07tic. Note that aging by O_3 in this
233 study refers to the reactions in which O_3 oxidized the remaining double bonds for precursors with
234 multiple double bonds. Due to a lack of evidence regarding SOA mass increase through
235 multigenerational oxidation with NO_3 radical, it was not considered in the model. SVOC with a
236 high volatility in the two-product model, denoted as HSVOC, reacted with oxidants, evolving into
237 the corresponding SVOC with a low volatility (LSVOC). LSVOC was oxidized to form ASVOC
238 with the vapor pressure decreasing further. For species with a fixed SOA yield, e.g. limonene, the
239 respective oxidation product was not subject to multigenerational oxidation given that it was
240 non-volatile. At each computation timestep, HSVOC and LSVOC were limited to one oxidation
241 step. Additionally, ASVOCs were assumed to be non-volatile, which would not partition back to
242 the gas phase, with carbon mass conserved and the same OM/OC ratio (2.1) as oligomers in
243 current CMAQ. Other chemical aging processes such as photolysis and fragmentation in the
244 condensed phase, which will decrease the aerosol mass, were not considered (Donahue et al.,
245 2012a; Jathar et al., 2015). Therefore, the simulated OA concentration with multigenerational
246 oxidation may be an upper limit and was investigated using a sensitivity analysis calculation.

247 **3. Results and discussion**

3.1. Model performance

CMAQ performance for gases CO, NO$_2$, and aerosol components (sulfate, nitrate, ammonium, EC, and OC) in the three cases (i.e. the base, detailed and aging case) was examined by comparing the simulations to observations at CTR (see the performance metrics shown in Table S3). Diurnal patterns of simulated individual monoterpenes against observations are shown in Fig.1, with oxidants including hydroxyl radical, O$_3$, nitrate radical, and gas-phase organonitrates shown in Fig.3.

3.1.1. Major gases and aerosols

There were no significant differences among the three cases for the simulated species except OC, which showed enhanced performance due to updated representations of BSOA with the detailed and aging models. CO was biased low by ~30%, and simulated average concentration of NO$_2$ during the SOAS was almost in line with the observation at rural CTR. CMAQ reproduced 80-90% of observed sulfate and 50-60% of ammonium, but it failed to capture nitrate, which is quite low in warm seasons. The low bias in nitrate is partly explained by model biases in ammonia and sulfate as also found by Yu et al. (2005). Further, the underestimation of nitric acid (Fig. S9) is linked to a high bias in organic nitrate of about the same magnitude (Fig.3) suggesting that there is an overabundance of organic radical formation. This is tied to reactions of isoprene in the presence of NO$_x$ as discussed in Section 3.1.3. Low bias was also shown for EC, likely related to biomass burning, whose emissions were not fully captured in the model. The negative bias of OC changed from -64% for the base case to -43% in the detailed case. By implementing multigenerational oxidation, OC was biased high (normalized mean bias (NMB) of ~20%). According to the recommended benchmarks for performance statistics (Emery et al., 2017), criteria for normalized mean error (NME) and correlation coefficient (r) of speciated aerosol were met, while NMBs of ammonium, nitrate, and EC were violated (marked in red in Table S3).

3.1.2. Monoterpenes

Base case simulated monoterpene, specifically α-pinene and other monoterpenes (APIN and TERP in the standard SARPRC07tic mechanism) concentrations, show more pronounced diurnal trends than the measurements (Fig. S1). Model biases for speciated monoterpenes were examined by using the base biogenic inventory except individual monoterpene emissions had not been merged in BEIS3, along with the detailed model (referred to as "Detailed (base emission)" in Fig.1). It is expected that simulated "other" monoterpenes (lower right corner of Fig.1) was likely biased high because only measurements of myrcene and camphene were available, while the simulation in the base case included more species. However, high biases of the individual monoterpene (~2x for α-pinene and limonene and ~1.5x for β-pinene on average during 18:00-6:00) were found, though simulated daytime concentrations of β-pinene and limonene were less than half of the observations (Fig.1). The influence of the shallow boundary layer on the elevated mixing ratio of monoterpenes at night was found to be minimal in simulations by Vasilakos (2018), and simulated CO did not show an excessive build up at night either (Fig. S2). Also, model biases of oxidants, such as high bias of O$_3$ (Fig. 3), hardly affected the simulated monoterpenes given that biogenic VOCs were abundant at CTR (discussed in Section 3.3), and only a small quantity of monoterpenes was consumed by reactions with oxidants locally. This

289   suggests that the inability to reproduce observed monoterpenes is linked to emissions.

290   The emission profiles of α-pinene, β-pinene, and limonene were modified. The modified diurnal
291   emissions variation leads to increased emissions during the day (Fig. 2). This supports a
292   possibility of a direct response to photosynthetically active radiation (PAR), but is not direct
293   evidence. This can also be attributed to uncertainties in the emissions model response to
294   temperature and local heating from solar radiation. Monoterpene emissions estimated by BEIS3
295   are assumed to increase exponentially with temperature with an exponential factor of 0.09,
296   slightly lower than that applied to the Model of Emissions of Gases and Aerosols from Nature
297   version 2.1 (MEGAN2.1), which is 0.1 (Guenther et al., 2012; Pouliot and Pierce, 2009).
298   Adjusting emissions to best capture the observed gas-phase concentrations of those compounds
299   led to the NMB, for hourly monoterpene concentrations, being reduced from 13-160% to 1-45%
300   with higher correlations in both the detailed and aging case (Fig. 1; simulated monoterpene
301   concentrations in the aging case were very close to the detailed case and thus not shown).
302   Therefore, adjusting emissions possibly reduces the influence of biased emissions on the
303   simulated SOA_M.

304   3.1.3. Hydroxyl radical, O_3, nitrate radical and gas-phase organonitrates

305   Simulated OH radical concentrations were in line with the observations in the base and detailed
306   cases (Fig. 3). Increased emission rates of monoterpenes with the detailed model slightly
307   decreased OH radical peak values slightly. The aging model obtained almost the same level of
308   oxidants as in the detailed case (Table 1) due to the assumption that the aerosol aging processes
309   do not consume a significant amount of gas phase oxidants in the model. Observed O_3 levels
310   were low during this period, averaging only ~26ppb; the simulated O_3 levels were also low,
311   though they were biased high by ~9ppb, corresponding to NMB of 34-35% (Table 1). The
312   detailed and aging models had a minor effect on simulated OH radical and O_3. However, the
313   simulated NO_3 increased during the night, from a tendency towards a low bias (−18.3%) to a
314   high bias (48.3%) compared to NO_3 $_{SS}$. As indicated by Ayres et al. (2015), reactions with
315   monoterpenes were the dominant sink of NO_3 radical at CTR at night, and the high monoterpene
316   levels suppressed NO_3. With the reduction of simulated nocturnal monoterpene emissions, the
317   negative model biases in the early morning decreased in the detailed case with a simulated peak
318   of ~2ppt at 5:00 a.m., and NO_3 in the late evening was biased high by a factor of 2.

319   Compared to the base case, simulated gas-phase organonitrates increased by ~10% with the
320   updated monoterpene description (both emissions and gas-phase chemistry). The percentage was
321   small relative to the increase in daytime monoterpene emissions (Fig.2), suggesting a limited
322   contribution of monoterpenes to gas-phase organonitrates, with isoprene being a more important
323   contributor (anthropogenic VOCs were low at CTR). A fraction of monoterpene-formed
324   organonitrates, which are supposed to condense onto particles and become part of BSOA,
325   remained in the gas phase in the model. However, its effect on high bias of gas-phase
326   organonitrates (~90%) was minor. The elevated concentration around 10:00 a.m. indicated
327   oxidations in the presence of NO_x could be mainly responsible for the production of gas-phase
328   organonitrates, instead of nitrate radical chemistry. Therefore, high bias of gas-phase
329   organonitrates might result from overestimated formation of organonitrates from high NO_x

330   photooxidation in the model.

3.2. Simulated organic aerosols

332   Organic aerosols were biased low, more so in the base case (~ -50%) than the detailed case with
333   updated yields of monoterpene + NO_3 (~ -20%; Fig. 4 (a) and Table 1). One reason for the low
334   bias was that highly variable and uncertain primary emissions, such as from biomass burning,
335   were not fully captured. This was examined by comparing model biases for EC versus OC, and
336   CO versus OC (Fig. S3), as emissions of CO and EC are substantial for biomass burning (Geddes
337   et al., 2016; Heald and Geddes, 2016; Zhang and Wang, 2016), and prescribed fires are common
338   in the SE US (Garcia‑Menendez et al., 2013; Odman et al., 2014; Penkett et al., 2007). When
339   simulated OC was low, EC and CO were typically also biased low, suggesting a potential
340   influence of biomass burning on OC simulation. For better comparison, we subtracted the
341   biomass burning OA (BBOA) from the total measured OA (gray line in Fig. 4 (a)). Note that the
342   calculated BBOA likely represents the relatively fresh OA from biomass burning, while aged OA
343   from biomass burning is apportioned to the MO-OOA (Xu et al., 2015b). Aged BBOA missing
344   from the model could partly explain the observation-simulation gap in the detailed case, even
345   though BBOA had been excluded from the observation. The observation-model agreement of the
346   detailed model improved compared to the baseline, with the simulated OA increasing from 2.25
347   to 3.40 $\mu g \cdot m^{-3}$ at night (20:00-6:00 Local Time) mainly due to the updated yield. The daytime
348   concentration increased from 2.07 to 2.76 $\mu g \cdot m^{-3}$ due to the adjustment of emissions. The high
349   bias of SOA_I was one of the reasons the simulated OA was ~70% higher than the observation
350   with the aging model (Fig. S4). By excluding SOA_I from either the simulated or observed OA,
351   the positive bias of the aging model decreased to ~40% (Fig.4 (c) and Table 1).

352   Xu et al. (2015a) proposed that the PMF-identified subtype LO-OOA is likely related to
353   organonitrates, which is the primary component of SOA formed from monoterpene + NO_3. The
354   diurnal variations of LO-OOA and SOA_M were examined (Fig.4 (b)). In the detailed case, SOA_M
355   was responsible for approximately one-third of LO-OOA, with a substantial fraction (~80% on
356   average) of SOA_M coming from monoterpene + NO_3 at night when high levels of LO-OOA and
357   simulated SOA_M occurred (Fig. 4 (b)). Fry et al. (2014) found that the fraction of total aerosol
358   mass produced by the NO_3 chemistry due to organonitrates ranges from 56-82% for varied
359   terpene species. If this were true, organonitrates originating from monoterpene + NO_3 would
360   account for 15-26% of LO-OOA. However, based on the report from Xu et al. (2015a) that 15-26%
361   of LO-OOA is contributed by organonitrates in the early morning, and the assumption that 65%
362   of organonitrates is from monoterpenes according to Lee et al. (2016), we roughly estimated that
363   13-20% of LO-OOA could be attributed to the reactions of monoterpenes with NO_3. The
364   contribution of monoterpene-formed organonitrates to LO-OOA in the detailed case (15-26%) is
365   similar to the observation-based estimation (13-20%).

366   By using the detailed model, negative biases for observed OA (without BBOA and isop_OA)
367   remained (Fig. 4(c)). Possible reasons include: (1) Negative biases of OA mass loading leads to
368   less SVOCs partitioning into the condensed phase, which is particularly the case when biomass
369   burning occurs; (2) Multigenerational oxidations of SVOCs are possibly suppressed in the
370   chamber experiments, leading to lower SOA yields measured. Thus, the influence of

371 multigenerational oxidation was investigated with the aging model. Simulated OA (without SOA_I)
372 was greatly enhanced by incorporating multigenerational oxidation of SVOCs into CMAQ, and
373 this level can be comparable to the sum of MO-OOA and LO-OOA (Fig. 4 (c) (d)). MO-OOA
374 has the highest OM:OC ratio (2.47) among the four OA factors identified at CTR. There is
375 observational evidence that MO-OOA shows correlation with O_3 in summer in the SE US, with
376 the oxidation of biogenic VOCs serving as a source of summertime MO-OOA in this region (Xu
377 et al., 2015b). In the aging case simulation, ASVOCs with OM:OC ratio (2.1) presumed in the
378 model were less oxygenated than observed MO-OOA. ASVOCs predominantly originated from
379 monoterpenes which accounted for ~70% (Fig. 4(d)) at CTR. The aging model captured
380 pollution events with high levels of OA. In a few cases, elevated OA was simulated, but the
381 observation did not increase as much. The simulated OA concentration at CTR during the SOAS
382 campaign was 4.1 $\mu g \cdot m^{-3}$ on average, with 2.7 $\mu g \cdot m^{-3}$ from multigenerational oxidation
383 processes, and OA was biased high by 36% compared to the observation.

384 The positive biases of OA (Fig. 4(c)) were more significant at night, implying that initial OA
385 contributed by monoterpene + NO_3 could be overestimated. For example, "other" monoterpenes
386 using the yield of β-pinene + NO_3, might not produce SOA as efficiently as β-pinene. More
387 importantly, the SOA yield for limonene + NO_3 applied in the detailed and aging models was
388 obtained assuming that NO_3 radical oxidized both double bonds of limonene (Boyd et al., 2017),
389 but this was not the case at CTR due to abundant BVOCs, as discussed in Section 3.3. With
390 combined oxidation by NO_3 and O_3, SOA yield could be lower, e.g. ~40% at a mass loading of
391 10 $\mu g \cdot m^{-3}$ (Fry et al., 2011). The 16-day test using SOA yield for limonene + NO_3 of 40%, with
392 the assumption that SOA formed from this pathway is non-volatile (the yield curve was not
393 available), showed that the simulated OA without SOA_I decreased from 4.1 to 3.8 $\mu g \cdot m^{-3}$ at
394 night (indicated as *Lim40* in Fig. S5), with the NMB decreasing from 19% to 11%.

395 Two additional tests (indicated as *Half* and *No_O3* in Fig.S5) were conducted. One was
396 motivated by the conjecture that SVOCs react with O_3/OH at a lower reaction rate than the
397 precursor VOC. For instance, this was true for either the first generation products of isoprene
398 reacting with OH (i.e. hydroxyhydroperoxides (ISOPOOH) or methacrolein (MACR)) compared
399 to isoprene (Xu et al., 2014), or the oxidation products of α-pinene + OH (Eddingsaas et al.,
400 2012). A 50% reduction in the aging rates of SVOCs corresponded to ~30% decrease of
401 ASVOCs and resulted in almost the same level of mean OA concentration as the observation at
402 CTR. However, it cannot explain the severe overestimation at certain times (June 11 through
403 June 13) since the time series did not change significantly with the correlation coefficient like
404 that in the aging case. The other test eliminated O_3 aging in the aging model since the oxidation
405 products of VOCs might lack a double bond limiting their reaction with O_3 (Palm et al., 2017).
406 With O_3 aging not considered, ASVOCs decreased ~0.4 $\mu g \cdot m^{-3}$, suggesting that O_3 aging only
407 accounted for a small fraction (~20%) of ASVOCs in the aging case while OH oxidation
408 dominated the aging processes. High biases, with NMB of 8%, for simulated OA remained even
409 with no O_3 aging. Other aging processes such as fragmentation and photolysis were not
410 investigated in this work which might also contribute to high biases of OA.

411 **3.3. Contribution to SOA_M**

412 The spatial distribution of BSOA formed from monoterpene via various oxidation pathways (Fig.
413 5 (a) (b)) shows that SOA_M was predominantly from reactions with NO_3 radical due to the high
414 aerosol yield. Nitrate radical chemistry produced up to ~0.9 $\mu g \cdot m^{-3}$ BSOA, three times as much
415 as that from oxidations by oxidants dominant during the day (e.g. O_3 and OH). The spatial
416 patterns of the two pathways were similar, with an elevated concentration in the southern and
417 southeastern US, co-located with emission sources. When multigenerational oxidation was
418 considered, ASVOCs became a critical component of SOA_M (Fig. 5(c)). They spread widely and
419 showed different spatial variation from the initial SOA_M. The simulation without O_3 aging
420 (*No_O3*) yielded a similar spatial distribution of ASVOCs (Fig. S7), suggesting that it should not
421 be determined by O_3 concentration. It could not be associated with OH radical either, due to
422 different spatial pattern between OH and ASVOCs. Therefore, the accumulation of ASVOCs
423 could likely be driven by meteorology or long-range transport. Compared to the simulation
424 conducted by Pye et al. (2015) (Figure 1 (a) (c) in that paper), initial SOA_M from nitrate radical
425 chemistry in this work was lower by a factor of ~2, but it was comparable to the estimation in
426 Pye et al. (2015) when ASVOCs were included.

427 While the focus of this manuscript was on simulating monoterpene SOA formation in the
428 Southeast, inclusion of the multigenerational aging of terpene-related species leads to a high bias
429 in the Southwest US, in and downwind of regions with high monoterpene emissions (Fig. S11).
430 Recent work using satellite HCHO retrievals and model inversion methods by Kaiser et al. (2017)
431 has found a high bias in emissions in Texas linked to a factor of about three high bias in isoprene
432 emissions due to land use classification issues, which could also lead to biases in terpene
433 emissions.   Examination of satellite photos of the area with high terpene emissions shows it to
434 be relatively barren, with patches of agriculture. The dominance of terpene-related oxidation
435 products contributing to SOA, versus isoprene or fungal spores, in the Southwest are consistent
436 with detailed chemical characterization of contemporary carbon in the SOA (Schictel et al., 2008;
437 Holden et al., 2011). Further studies of biogenic SOA formation in the Southwest are underway.

438 The total loss rate of various monoterpenes to oxidants was simulated to be in the range of
439 0.21-0.34 $ppb \cdot h^{-1}$ at CTR (Fig. 6 (a) (b)), one or two orders of magnitudes lower than the
440 estimated total emission rate. For instance, the emission rate of 0.01-0.13 $mole \cdot s^{-1} \cdot km^{-2}$ for
441 α-pinene (Fig. 2) was equivalent to 1-20 $ppb \cdot h^{-1}$ presuming the boundary layer height (BLH)
442 was in the range of 500-1500m. Oxidants depleted a small fraction of emitted BVOCs suggesting
443 CTR remained in the oxidant-sensitive regime. The large abundance of BVOCs suppressed the
444 oxidant levels. Depletion of monoterpenes was dominated by O_3 and OH oxidations during the
445 daytime, tending to peak from 7:00-15:00 Local Time. At night (20:00-5:00 Local Time),
446 reaction with NO_3 increased in importance, making up ~22% of monoterpene losses (Fig. S8 (a)),
447 specifically 23% of α-pinene losses and 29% of β-pinene losses. This was in line with the
448 estimated reaction branching ratio of monoterpene with respect to O_3 versus NO_3 based on
449 measurements at CTR which is 0.21 for α-pinene + NO_3 and 0.38 for β-pinene + NO_3,
450 respectively (Xu et al., 2015a).

451 The contributions of individual monoterpene via various oxidation pathways to SOA_M formation
452 (Fig. 6 (c) (d) (e)) were quite different in comparison to loss rates. Even at night when NO_3

453 concentrations built up, O_3 still dominated monoterpene oxidation at CTR, while the lower
454 aerosol yield for reactions with O_3 weakened the role of O_3 oxidation in SOA_M production. O_3
455 and OH radical oxidation produced a total of ~0.2 $\mu g \cdot m^{-3}$ aerosol masses corresponding to ~9%
456 of SOA_M (Fig. S8 (b)), nearly half of the amount derived from NO_3 oxidation (~18% of SOA_M).
457 On average, limonene contributed 53% to SOA_M formed from nitrate radical chemistry, up to 0.5
458 $\mu g \cdot m^{-3}$ in the early morning, followed by β-pinene reactions that contributed 28%. ASVOCs
459 were the dominant component of SOA_M, maintaining over 1.5 $\mu g \cdot m^{-3}$ and peaking in the
460 afternoon.

461 **4. Conclusions**

462 Monoterpene reactions with NO_3 were found to be responsible for most of the OA production at
463 night during the SOAS campaign. However, CMAQ historically has found simulated OA levels
464 biased low during the summer, and part of this bias was found to be due to a low bias in the
465 formation of OA from monoterpene-NO_3 reactions. In this study, CMAQ was extended to
466 include updated species-specific emissions, reactions, aerosol yields, and partitioning parameters
467 of monoterpenes. Particularly, the extension included updated yields for nitrate radical chemistry
468 (which is particularly important at night), instead of those based on daylight experimental data.
469 Biogenic emissions calculated online with BEIS3 were also constrained using species-specific
470 observations. With the more detailed model, simulated OA increased by ~1 $\mu g \cdot m^{-3}$ on average,
471 reproducing ~80% of the observed OA (without BBOA) at CTR. Simulated
472 monoterpene-derived BSOA constituted one-third of LO-OOA at night and showed a more
473 consistent diurnal pattern than the baseline. By implementing a multigenerational oxidation
474 scheme, the gap between measurements and simulation was further reduced, and the model
475 simulated elevated OA episodes, comparable to the measurements (LO-OOA + MO-OOA), with
476 a high bias of 36%. Aged SVOCs were the dominant components of monoterpene-derived BSOA,
477 contributing over 1.5 $\mu g \cdot m^{-3}$ (>60%) on average, underscoring the important role that
478 multigenerational oxidation may play in SOA formation. Initial SOA via nitrate radical chemistry
479 contributed up to 34% at night. However, with a biased high of the simulated OA concentration,
480 aerosol productions in the aging model may represent an upper limit of the SOA formation from
481 the multigenerational oxidation.

482 This work revealed that updating SOA yields for monoterpene + NO_3 reactions with recent
483 experimental data (e.g. for β-pinene/limonene + NO_3) increases simulated OA at night as seen in
484 observations, particularly in locations with abundant BVOCs interacting with anthropogenic
485 emissions. However, it calls for more chamber studies exploring BSOA formation from other
486 monoterpenes. Additionally, aerosol yields for reactions of monoterpene with O_3/OH in the
487 model were outdated and should be updated at lower OA mass loadings, more relevant to the real
488 atmosphere. Implementing multigenerational-oxidation of BVOC + NO_3 chemistry is
489 recommended, in line with recent chemistry analyses and field observations. This work also
490 found that the diurnal emission profile by BEIS did not produce observed BVOCs and that more
491 examination is warranted.

492 **Acknowledgement**

505 **Reference**

506 Allen, H.M., Draper, D.C., Ayres, B.R., Ault, A., Bondy, A., Takahama, S., Modini, R.L., Baumann,
507 K., Edgerton, E., Knote, C., 2015. Influence of crustal dust and sea spray supermicron particle
508 concentrations and acidity on inorganic NO 3– aerosol during the 2013 Southern Oxidant and Aerosol
509 Study. Atmospheric Chemistry and Physics 15, 10669-10685.

510 Atkinson, R., Arey, J., 2003. Gas-phase tropospheric chemistry of biogenic volatile organic
511 compounds: a review. Atmospheric Environment 37, S197-S219.

512 Aumont, B., Valorso, R., Mouchel-Vallon, C., Camredon, M., Lee-Taylor, J., Madronich, S., 2012.
513 Modeling SOA formation from the oxidation of intermediate volatility n-alkanes. Atmospheric
514 Chemistry and Physics 12, 7577-7589.

515 Ayres, B., Allen, H., Draper, D., Brown, S., Wild, R., Jimenez, J., Day, D., Campuzano-Jost, P., Hu,
516 W., Gouw, J.d., 2015. Organic nitrate aerosol formation via NO 3+ biogenic volatile organic
517 compounds in the southeastern United States. Atmospheric Chemistry and Physics 15, 13377-13392.

518 Baek, J., Hu, Y., Odman, M.T., Russell, A.G., 2011. Modeling secondary organic aerosol in CMAQ
519 using multigenerational oxidation of semi‐volatile organic compounds. Journal of Geophysical
520 Research: Atmospheres (1984–2012) 116.

521 Boyd, C.M., Nah, T., Xu, L., Berkemeier, T., Ng, N.L., 2017. Secondary Organic Aerosol (SOA) from
522 Nitrate Radical Oxidation of Monoterpenes: Effects of Temperature, Dilution, and Humidity on
523 Aerosol Formation, Mixing, and Evaporation. Environmental Science & Technology 51, 7831-7841.

524 Boyd, C.M., Sanchez, J., Xu, L., Eugene, A.J., Nah, T., Tuet, W.Y., Guzman, M.I., Ng, N.L., 2015.
525 Secondary organic aerosol formation from the β-pinene+NO$_3$ system: effect of humidity and peroxy
526 radical fate. Atmospheric Chemistry and Physics 15, 7497-7522.

527 Brophy, P., Farmer, D., 2015. A switchable reagent ion high resolution time-of-flight chemical
528 ionization mass spectrometer for real-time measurement of gas phase oxidized species:
529 characterization from the 2013 southern oxidant and aerosol study. Atmospheric Measurement
530 Techniques 8, 2945-2959.

531 Byun, D., Schere, K., 2006. Review of the Governing Equations, Computational Algorithms, and
532 Other Components of the Models-3 Community Multiscale Air Quality (CMAQ) Modeling System.
533 Applied Mechanics Reviews 59, 51-77.

534 Carlton, A., Goldstein, A., Jimenez, J., Pinder, R., DeGouw, J., Turpin, B., Guenther, A., Cohen, R.,
535 Shepson, P., Shaw, S., 2013. The Southern Oxidant and Aerosol Study (SOAS): Measuring and
536 modeling at the interface of air quality and climate change to understand biosphere-atmosphere
537 interactions [White Paper]. Retrieved October.

538 Carlton, A.G., Bhave, P.V., Napelenok, S.L., Edney, E.O., Sarwar, G., Pinder, R.W., Pouliot, G.A.,
539 Houyoux, M., 2010. Model representation of secondary organic aerosol in CMAQv4. 7.
540 Environmental science & technology 44, 8553-8560.

541 Carter, W.P., 2010a. Development of the SAPRC-07 chemical mechanism. Atmospheric Environment
542 44, 5324-5335.

543 Carter, W.P., 2010b. Development of the SAPRC-07 chemical mechanism and updated ozone
544 reactivity scales, Report to the California Air Resources Board, Contract No. 03–18, 06-408, and
545 07-730, 27 January 2010 (available at: http://www.engr.ucr.edu/carter/SAPRC/), 2010.

546 Chen, Q., Heald, C.L., Jimenez, J.L., Canagaratna, M.R., Zhang, Q., He, L.Y., Huang, X.F.,
547 Campuzano‐Jost, P., Palm, B.B., Poulain, L., 2015. Elemental composition of organic aerosol: The
548 gap between ambient and laboratory measurements. Geophysical Research Letters 42, 4182-4189.

549   Donahue, N.M., Epstein, S., Pandis, S.N., Robinson, A.L., 2011. A two-dimensional volatility basis
550   set: 1. organic-aerosol mixing thermodynamics. Atmospheric Chemistry and Physics 11, 3303-3318.
551   Donahue, N.M., Henry, K.M., Mentel, T.F., Kiendler-Scharr, A., Spindler, C., Bohn, B., Brauers, T.,
552   Dorn, H.P., Fuchs, H., Tillmann, R., 2012a. Aging of biogenic secondary organic aerosol via
553   gas-phase OH radical reactions. Proceedings of the National Academy of Sciences 109, 13503-13508.
554   Donahue, N.M., Kroll, J., Pandis, S.N., Robinson, A.L., 2012b. A two-dimensional volatility basis
555   set–Part 2: Diagnostics of organic-aerosol evolution. Atmospheric Chemistry and Physics 12,
556   615-634.
557   Eddingsaas, N., Loza, C., Yee, L., Seinfeld, J., Wennberg, P., 2012. α-pinene photooxidation under
558   controlled chemical conditions–Part 1: Gas-phase composition in low-and high-NO x environments.
559   Atmospheric Chemistry and Physics 12, 6489-6504.
560   Edgerton, E.S., Hartsell, B.E., Saylor, R.D., Jansen, J.J., Hansen, D.A., Hidy, G.M., 2005. The
561   Southeastern Aerosol Research and Characterization Study: Part II. Filter-based measurements of fine
562   and coarse particulate matter mass and composition. Journal of the Air & Waste Management
563   Association 55, 1527-1542.
564   Edgerton, E.S., Hartsell, B.E., Saylor, R.D., Jansen, J.J., Hansen, D.A., Hidy, G.M., 2006. The
565   Southeastern Aerosol Research and Characterization Study, part 3: Continuous measurements of fine
566   particulate matter mass and composition. Journal of the Air & Waste Management Association 56,
567   1325-1341.
568   Emery, C., Liu, Z., Russell, A.G., Odman, M.T., Yarwood, G., Kumar, N., 2017. Recommendations on
569   statistics and benchmarks to assess photochemical model performance. Journal of the Air & Waste
570   Management Association 67, 582-598.
571   Fry, J., Kiendler-Scharr, A., Rollins, A., Brauers, T., Brown, S., Dorn, H.-P., Dubé, W., Fuchs, H.,
572   Mensah, A., Rohrer, F., 2011. SOA from limonene: role of NO_3 in its generation and degradation.
573   Atmospheric Chemistry and Physics 11, 3879-3894.
574   Fry, J., Kiendler-Scharr, A., Rollins, A., Wooldridge, P., Brown, S., Fuchs, H., Dubé, W., Mensah, A.,
575   Maso, M.d., Tillmann, R., 2009. Organic nitrate and secondary organic aerosol yield from NO_3
576   oxidation of β-pinene evaluated using a gas-phase kinetics/aerosol partitioning model. Atmospheric
577   Chemistry and Physics 9, 1431-1449.
578   Fry, J.L., Draper, D.C., Barsanti, K.C., Smith, J.N., Ortega, J., Winkle, P.M., Lawler, M.J., Brown,
579   S.S., Edwards, P.M., Cohen, R.C., Lee, L., 2014. Secondary Organic Aerosol Formation and Organic
580   Nitrate Yield from NO3 Oxidation of Biogenic Hydrocarbons. Environmental Science & Technology
581   48, 11944-11953.
582   Garcia‐Menendez, F., Hu, Y., Odman, M.T., 2013. Simulating smoke transport from wildland fires
583   with a regional‐scale air quality model: Sensitivity to uncertain wind fields. J. Geophys. Res., Atmos.
584   118, 6493-6504.
585   Geddes, J.A., Heald, C.L., Silva, S.J., Martin, R.V., 2016. Land cover change impacts on atmospheric
586   chemistry: simulating projected large-scale tree mortality in the United States. Atmospheric
587   Chemistry and Physics 16, 2323-2340.
588   Griffin, R.J., Cocker, D.R., Flagan, R.C., Seinfeld, J.H., 1999. Organic aerosol formation from the
589   oxidation of biogenic hydrocarbons. Journal of Geophysical Research-Atmospheres 104, 3555-3567.
590   Guenther, A., Jiang, X., Heald, C., Sakulyanontvittaya, T., Duhl, T., Emmons, L., Wang, X., 2012.
591   The Model of Emissions of Gases and Aerosols from Nature version 2.1 (MEGAN2. 1): an extended
592   and updated framework for modeling biogenic emissions.

593   Hallquist, M., Wängberg, I., Ljungström, E., Barnes, I., Becker, K.-H., 1999. Aerosol and product
594   yields from NO₃ radical-initiated oxidation of selected monoterpenes. Environmental science &
595   technology 33, 553-559.
596   Hallquist, M., Wenger, J., Baltensperger, U., Rudich, Y., Simpson, D., Claeys, M., Dommen, J.,
597   Donahue, N., George, C., Goldstein, A., 2009. The formation, properties and impact of secondary
598   organic aerosol: current and emerging issues. Atmospheric Chemistry and Physics 9, 5155-5236.
599   Hansen, D.A., Edgerton, E.S., Hartsell, B.E., Jansen, J.J., Kandasamy, N., Hidy, G.M., Blanchard,
600   C.L., 2003. The southeastern aerosol research and characterization study: part 1—overview. Journal
601   of the Air & Waste Management Association 53, 1460-1471.
602   Hayes, P., Carlton, A., Baker, K., Ahmadov, R., Washenfelder, R., Alvarez, S., Rappenglück, B.,
603   Gilman, J., Kuster, W., de Gouw, J., 2015. Modeling the formation and aging of secondary organic
604   aerosols in Los Angeles during CalNex 2010. Atmospheric chemistry and physics 15, 5773-5801.
605   Heald, C.L., Geddes, J.A., 2016. The impact of historical land use change from 1850 to 2000 on
606   secondary particulate matter and ozone. Atmospheric Chemistry and Physics 16, 14997-15010.
607   Henry, K.M., Donahue, N.M., 2012. Photochemical Aging of α-Pinene Secondary Organic Aerosol:
608   Effects of OH Radical Sources and Photolysis. The Journal of Physical Chemistry A 116, 5932-5940.
609   Holden, A.S., Sullivan, A.P., Munchak, L.A., Kreidenweis, S.M., Schichtel, B.A., Malm, W.C., Collett
610   Jr, J.L., 2011. Determining contributions of biomass burning and other sources to fine particle
611   contemporary carbon in the western United States. Atmospheric environment 45, 1986-1993.
612   Houyoux, M.R., Vukovich, J.M., 1999. Updates to the Sparse Matrix Operator Kernel Emissions
613   (SMOKE) modeling system and integration with Models-3. The Emission Inventory: Regional
614   Strategies for the Future 1461.
615   Hu, Y.T., Odman, M.T., Chang, M.E., Russell, A.G., 2015. Operational forecasting of source impacts
616   for dynamic air quality management. Atmospheric Environment 116, 320-322.
617   Jathar, S.H., Cappa, C.D., Wexler, A.S., Seinfeld, J.H., Kleeman, M.J., 2015. Multi-generational
618   oxidation model to simulate secondary organic aerosol in a 3-D air quality model. Geosci. Model Dev.
619   8, 2553-2567.
620   Jathar, S.H., Cappa, C.D., Wexler, A.S., Seinfeld, J.H., Kleeman, M.J., 2016. Simulating secondary
621   organic aerosol in a regional air quality model using the statistical oxidation model - Part 1: Assessing
622   the influence of constrained multi-generational ageing. Atmospheric Chemistry and Physics 16,
623   2309-2322.
624   Kaiser, J., Jacob, D.J., Zhu, L., Travis, K.R., Fisher, J.A., Abad, G.G., Zhang, L., Zhang, X., Fried, A.,
625   Crounse, J.D., 2017. High-resolution inversion of OMI formaldehyde columns to quantify isoprene
626   emission on ecosystem-relevant scales: application to the Southeast US.
627   Kleindienst, T.E., Jaoui, M., Lewandowski, M., Offenberg, J.H., Lewis, C.W., Bhave, P.V., Edney,
628   E.O., 2007. Estimates of the contributions of biogenic and anthropogenic hydrocarbons to secondary
629   organic aerosol at a southeastern US location. Atmospheric Environment 41, 8288-8300.
630   Koo, B., Knipping, E., Yarwood, G., 2014. 1.5-Dimensional volatility basis set approach for modeling
631   organic aerosol in CAMx and CMAQ. Atmospheric environment 95, 158-164.
632   Kroll, J.H., Ng, N.L., Murphy, S.M., Flagan, R.C., Seinfeld, J.H., 2006. Secondary organic aerosol
633   formation from isoprene photooxidation. Environmental science & technology 40, 1869-1877.
634   Kroll, J.H., Seinfeld, J.H., 2008. Chemistry of secondary organic aerosol: Formation and evolution of
635   low-volatility organics in the atmosphere. Atmospheric Environment 42, 3593-3624.
636   Kuwata, M., Liu, Y.J., McKinney, K., Martin, S.T., 2015. Physical state and acidity of inorganic

637   sulfate can regulate the production of secondary organic material from isoprene photooxidation
638   products. Physical Chemistry Chemical Physics 17, 5670-5678.

639   La, Y., Camredon, M., Ziemann, P., Valorso, R., Matsunaga, A., Lannuque, V., Lee-Taylor, J., Hodzic,
640   A., Madronich, S., Aumont, B., 2016. Impact of chamber wall loss of gaseous organic compounds on
641   secondary organic aerosol formation: explicit modeling of SOA formation from alkane and alkene
642   oxidation. Atmospheric Chemistry and Physics 16, 1417-1431.

643   Lee, B.H., Mohr, C., Lopez-Hilfiker, F.D., Lutz, A., Hallquist, M., Lee, L., Romer, P., Cohen, R.C.,
644   Iyer, S., Kurtén, T., 2016. Highly functionalized organic nitrates in the southeast United States:
645   Contribution to secondary organic aerosol and reactive nitrogen budgets. Proceedings of the National
646   Academy of Sciences 113, 1516-1521.

647   Li, J., Cleveland, M., Ziemba, L.D., Griffin, R.J., Barsanti, K.C., Pankow, J.F., Ying, Q., 2015.
648   Modeling regional secondary organic aerosol using the Master Chemical Mechanism. Atmospheric
649   Environment 102, 52-61.

650   Lin, Y.-H., Zhang, H., Pye, H.O., Zhang, Z., Marth, W.J., Park, S., Arashiro, M., Cui, T.,
651   Budisulistiorini, S.H., Sexton, K.G., 2013. Epoxide as a precursor to secondary organic aerosol
652   formation from isoprene photooxidation in the presence of nitrogen oxides. Proceedings of the
653   National Academy of Sciences 110, 6718-6723.

654   Liu, Y.J., Kuwata, M., Strick, B.F., Geiger, F.M., Thomson, R.J., McKinney, K.A., Martin, S.T., 2015.
655   Uptake of Epoxydiol Isomers Accounts for Half of the Particle-Phase Material Produced from
656   Isoprene Photooxidation via the HO2 Pathway. Environmental science & technology 49, 250-258.

657   Moldanova, J., Ljungström, E., 2000. Modelling of particle formation from NO_3 oxidation of selected
658   monoterpenes. Journal of aerosol science 31, 1317-1333.

659   Nah, T., McVay, R.C., Pierce, J.R., Seinfeld, J.H., Ng, N.L., 2017. Constraining uncertainties in
660   particle-wall deposition correction during SOA formation in chamber experiments. Atmospheric
661   Chemistry and Physics 17, 2297-2310.

662   Nah, T., McVay, R.C., Zhang, X., Boyd, C.M., Seinfeld, J.H., Ng, N.L., 2016. Influence of seed
663   aerosol surface area and oxidation rate on vapor wall deposition and SOA mass yields: a case study
664   with α-pinene ozonolysis. Atmospheric Chemistry and Physics 16, 9361-9379.

665   Nah, T., Sanchez, J., Boyd, C.M., Ng, N.L., 2015. Photochemical Aging of α-pinene and β-pinene
666   Secondary Organic Aerosol formed from Nitrate Radical Oxidation. Environmental science &
667   technology 50, 222-231.

668   Ng, N.L., Brown, S.S., Archibald, A.T., Atlas, E., Cohen, R.C., Crowley, J.N., Day, D.A., Donahue,
669   N.M., Fry, J.L., Fuchs, H., 2017. Nitrate radicals and biogenic volatile organic compounds: oxidation,
670   mechanisms, and organic aerosol. Atmospheric Chemistry and Physics 17, 2103-2162.

671   Nguyen, T., Petters, M., Suda, S., Guo, H., Weber, R., Carlton, A., 2014a. Trends in particle-phase
672   liquid water during the Southern Oxidant and Aerosol Study. Atmospheric Chemistry and Physics 14,
673   10911-10930.

674   Nguyen, T.B., Coggon, M.M., Bates, K.H., Zhang, X., Schwantes, R.H., Schilling, K.A., Loza, C.L.,
675   Flagan, R.C., Wennberg, P.O., Seinfeld, J.H., 2014b. Organic aerosol formation from the reactive
676   uptake of isoprene epoxydiols (IEPOX) onto non-acidified inorganic seeds. Atmospheric Chemistry
677   and Physics 14, 3497-3510.

678   Odman, M.T., Yano, A., Garcia-Menendez, F., Hu, Y., Goodrick, S.L., Liu, Y., Achtemeier, G.L., 2014.
679   Development and Evaluation of an Air Quality Model for Predicting the Impacts of Prescribed Burns,
680   Air Pollution Modeling and its Application XXII. Springer, pp. 517-521.

681 Odum, J.R., Hoffmann, T., Bowman, F., Collins, D., Flagan, R.C., Seinfeld, J.H., 1996. Gas/particle
682 partitioning and secondary organic aerosol yields. Environmental science & technology 30,
683 2580-2585.

684 Offenberg, J.H., Lewandowski, M., Jaoui, M., Kleindienst, T.E., 2011. Contributions of biogenic and
685 anthropogenic hydrocarbons to secondary organic aerosol during 2006 in Research Triangle Park, NC.
686 Aerosol and Air Quality Resarch 11, 99-108.

687 Paatero, P., Tapper, U., 1994. Positive matrix factorization: A non‐negative factor model with
688 optimal utilization of error estimates of data values. Environmetrics 5, 111-126.

689 Palm, B.B., Campuzano-Jost, P., Day, D.A., Ortega, A.M., Fry, J.L., Brown, S.S., Zarzana, K.J., Dube,
690 W., Wagner, N.L., Draper, D.C., 2017. Secondary organic aerosol formation from in situ OH, O 3, and
691 NO 3 oxidation of ambient forest air in an oxidation flow reactor. Atmospheric Chemistry and Physics
692 17, 5331-5354.

693 Palm, B.B., Campuzano-Jost, P., Ortega, A.M., Day, D.A., Kaser, L., Jud, W., Karl, T., Hansel, A.,
694 Hunter, J.F., Cross, E.S., 2016. In situ secondary organic aerosol formation from ambient pine forest
695 air using an oxidation flow reactor. Atmospheric Chemistry and Physics 16, 2943-2970.

696 Penkett, S., Burgess, R., Coe, H., Coll, I., Hov, Ø., Lindskog, A., Schmidbauer, N., Solberg, S.,
697 Roemer, M., Thijsse, T., 2007. Evidence for large average concentrations of the nitrate radical (NO 3)
698 in Western Europe from the HANSA hydrocarbon database. Atmospheric Environment 41,
699 3465-3478.

700 Perraud, V., Bruns, E.A., Ezell, M.J., Johnson, S.N., Greaves, J., Finlayson-Pitts, B.J., 2010.
701 Identification of organic nitrates in the NO3 radical initiated oxidation of α-pinene by atmospheric
702 pressure chemical ionization mass spectrometry. Environmental science & technology 44, 5887-5893.

703 Pouliot, G., Pierce, T., 2009. Integration of the Model of Emissions of Gases and Aerosols from
704 Nature (MEGAN) into the CMAQ Modeling System, 18th International Emission Inventory
705 Conference, Baltimore, Maryland, pp. 14-17.

706 Pye, H., Chan, A., Barkley, M., Seinfeld, J., 2010. Global modeling of organic aerosol: the importance
707 of reactive nitrogen (NOx and NO_3). Atmospheric Chemistry and Physics 10, 11261-11276.

708 Pye, H.O., Pinder, R.W., Piletic, I.R., Xie, Y., Capps, S.L., Lin, Y.-H., Surratt, J.D., Zhang, Z., Gold,
709 A., Luecken, D.J., 2013. Epoxide pathways improve model predictions of isoprene markers and
710 reveal key role of acidity in aerosol formation. Environmental science & technology 47,
711 11056-11064.

712 Pye, H.O.T., Luecken, D.J., Xu, L., Boyd, C.M., Ng, N.L., Baker, K.R., Ayres, B.R., Bash, J.,
713 Baumann, K., Carter, W.P., 2015. Modeling the current and future roles of particulate organic nitrates
714 in the southeastern United States. Environmental science & technology.

715 Rollins, A.W., Browne, E.C., Min, K.E., Pusede, S.E., Wooldridge, P.J., Gentner, D.R., Goldstein,
716 A.H., Liu, S., Day, D.A., Russell, L.M., Cohen, R.C., 2012. Evidence for NOx Control over
717 Nighttime SOA Formation. Science 337, 1210-1212.

718 Schichtel, B.A., Malm, W.C., Bench, G., Fallon, S., McDade, C.E., Chow, J.C., Watson, J.G., 2008.
719 Fossil and contemporary fine particulate carbon fractions at 12 rural and urban sites in the United
720 States. J. Geophys. Res., Atmos. 113.

721 Seinfeld, J.H., Pandis, S.N., 2012. Atmospheric chemistry and physics: from air pollution to climate
722 change. John Wiley & Sons.

723 Simon, H., Baker, K.R., Phillips, S., 2012. Compilation and interpretation of photochemical model
724 performance statistics published between 2006 and 2012. Atmospheric Environment 61, 124-139.

725 Skamarock, W.C., Klemp, J.B., Dudhia, J., Gill, D.O., Barker, D.M., Wang, W., Powers, J.G., 2005. A
726 description of the advanced research WRF version 2. DTIC Document.

727 Spittler, M., Barnes, I., Bejan, I., Brockmann, K., Benter, T., Wirtz, K., 2006. Reactions of NO$_3$
728 radicals with limonene and α-pinene: Product and SOA formation. Atmospheric Environment 40,
729 116-127.

730 Surratt, J.D., Chan, A.W.H., Eddingsaas, N.C., Chan, M.N., Loza, C.L., Kwan, A.J., Hersey, S.P.,
731 Flagan, R.C., Wennberg, P.O., Seinfeld, J.H., 2010. Reactive intermediates revealed in secondary
732 organic aerosol formation from isoprene. Proceedings of the National Academy of Sciences of the
733 United States of America 107, 6640-6645.

734 Surratt, J.D., Lewandowski, M., Offenberg, J.H., Jaoui, M., Kleindienst, T.E., Edney, E.O., Seinfeld,
735 J.H., 2007. Effect of acidity on secondary organic aerosol formation from isoprene. Environmental
736 science & technology 41, 5363-5369.

737 Surratt, J.D., Murphy, S.M., Kroll, J.H., Ng, N.L., Hildebrandt, L., Sorooshian, A., Szmigielski, R.,
738 Vermeylen, R., Maenhaut, W., Claeys, M., 2006. Chemical composition of secondary organic aerosol
739 formed from the photooxidation of isoprene. The Journal of Physical Chemistry A 110, 9665-9690.

740 Vasilakos, P., Pye, H., Hu, Y., Xu, L., Guo, H., Bougiatioti, A., Cerully, K., Goldstein, A., Guenther,
741 A., Ng, N.L., Surrat, J., Weber, R.W., Wennberg, P., Russell, A., Nenes, A., 2018. Constraining
742 IEPOX and IEPOX-derived SOA formation in CMAQ with the use of SOAS observations. in
743 preparation.

744 Weber, R.J., Sullivan, A.P., Peltier, R.E., Russell, A., Yan, B., Zheng, M., De Gouw, J., Warneke, C.,
745 Brock, C., Holloway, J.S., 2007. A study of secondary organic aerosol formation in the
746 anthropogenic-influenced southeastern United States. Journal of Geophysical Research: Atmospheres
747 (1984–2012) 112.

748 Worton, D.R., Surratt, J.D., LaFranchi, B.W., Chan, A.W., Zhao, Y., Weber, R.J., Park, J.-H., Gilman,
749 J.B., de Gouw, J., Park, C., 2013. Observational Insights into Aerosol Formation from Isoprene.
750 Environmental science & technology 47, 11403-11413.

751 Xie, Y., Paulot, F., Carter, W., Nolte, C., Luecken, D., Hutzell, W., Wennberg, P., Cohen, R., Pinder, R.,
752 2013. Understanding the impact of recent advances in isoprene photooxidation on simulations of
753 regional air quality. Atmospheric Chemistry and Physics 13, 8439-8455.

754 Xu, L., Guo, H., Boyd, C.M., Klein, M., Bougiatioti, A., Cerully, K.M., Hite, J.R.,
755 Isaacman-VanWertz, G., Kreisberg, N.M., Knote, C., Olson, K., Koss, A., Goldstein, A.H., Hering,
756 S.V., de Gouw, J., Baumann, K., Lee, S.-H., Nenes, A., Weber, R.J., Ng, N.L., 2015a. Effects of
757 anthropogenic emissions on aerosol formation from isoprene and monoterpenes in the southeastern
758 United States. Proceedings of the National Academy of Sciences of the United States of America 112,
759 37-42.

760 Xu, L., Kollman, M.S., Song, C., Shilling, J.E., Ng, N.L., 2014. Effects of NOx on the Volatility of
761 Secondary Organic Aerosol from Isoprene Photooxidation. Environmental science & technology 48,
762 2253-2262.

763 Xu, L., Suresh, S., Guo, H., Weber, R., Ng, N., 2015b. Aerosol characterization over the southeastern
764 United States using high resolution aerosol mass spectrometry: spatial and seasonal variation of
765 aerosol composition, sources, and organic nitrates. Atmospheric Chemistry and Physics Discussions
766 15, 10479-10552.

767 Yu, S., Bhave, P.V., Dennis, R.L., Mathur, R., 2007. Seasonal and regional variations of primary and
768 secondary organic aerosols over the continental United States: Semi-empirical estimates and model

769   evaluation. Environmental science & technology 41, 4690-4697.

770   Yu, S., Dennis, R., Roselle, S., Nenes, A., Walker, J., Eder, B., Schere, K., Swall, J., Robarge, W.,

771   2005. An assessment of the ability of three‑dimensional air quality models with current

772   thermodynamic equilibrium models to predict aerosol NO3−. J. Geophys. Res., Atmos. 110.

773   Zhang, X., Cappa, C.D., Jathar, S.H., McVay, R.C., Ensberg, J.J., Kleeman, M.J., Seinfeld, J.H., 2014.

774   Influence of vapor wall loss in laboratory chambers on yields of secondary organic aerosol.

775   Proceedings of the National Academy of Sciences 111, 5802-5807.

776   Zhang, Y.Z., Wang, Y.H., 2016. Climate-driven ground-level ozone extreme in the fall over the

777   Southeast United States. Proceedings of the National Academy of Sciences of the United States of
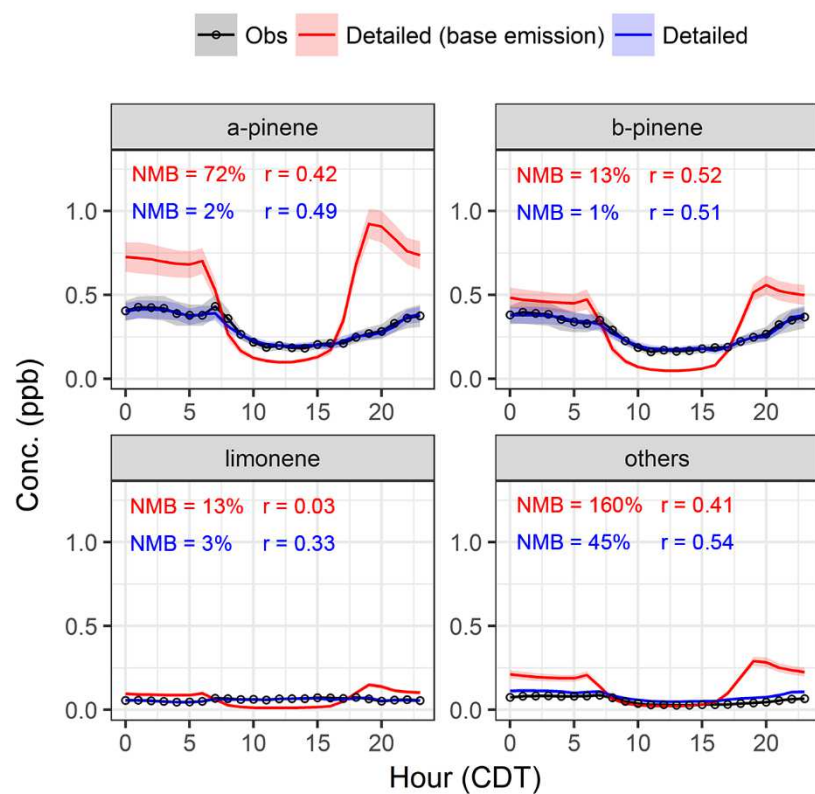
778   America 113, 10025-10030.

779

Fig.1 Diurnal trends of observed (black line) and simulated monoterpenes using the detailed model with base emissions (red line) and adjusted emissions (blue line) at Centreville during the SOAS campaign. The shaded area reflects a 95% Guassian confidence interval. Normalize mean bias (NMB) and correlation coefficient (r) are shown in the figure.
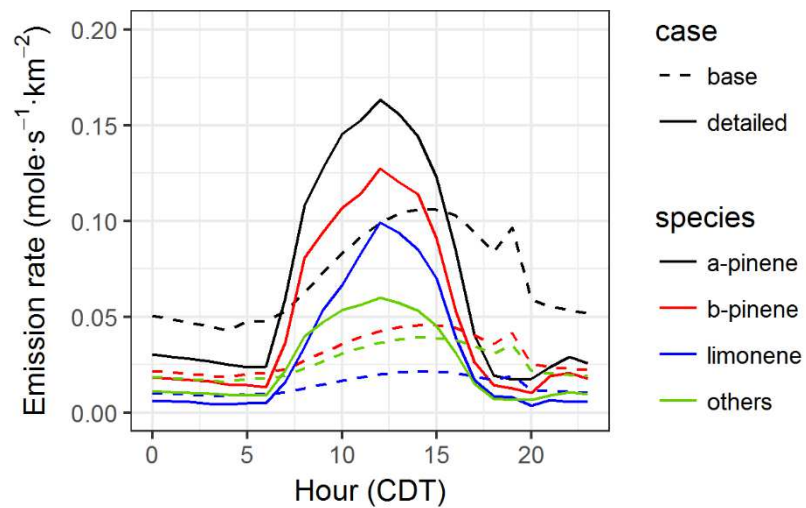
Fig. 2 Monoterpene emissions simulated online by default BEIS3 (dashed line) and simulation with modified diurnal emission profiles (solid line) at Centreville during the SOAS campaign.
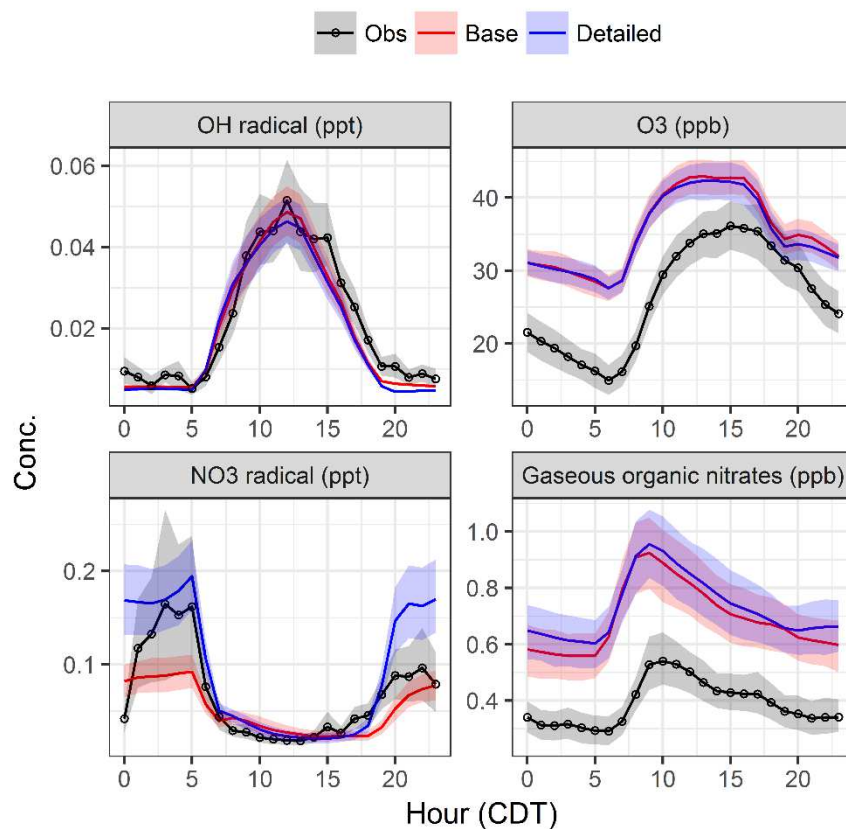
Fig. 3 Diurnal trends of observed (black line) and simulated oxidants (OH, O_3, NO_3), gas-phase organic nitrates with the base model (red line) and the detailed model (blue line) at Centreville during the SOAS campaign. The shaded area reflects a 95% Gaussian confidence interval.
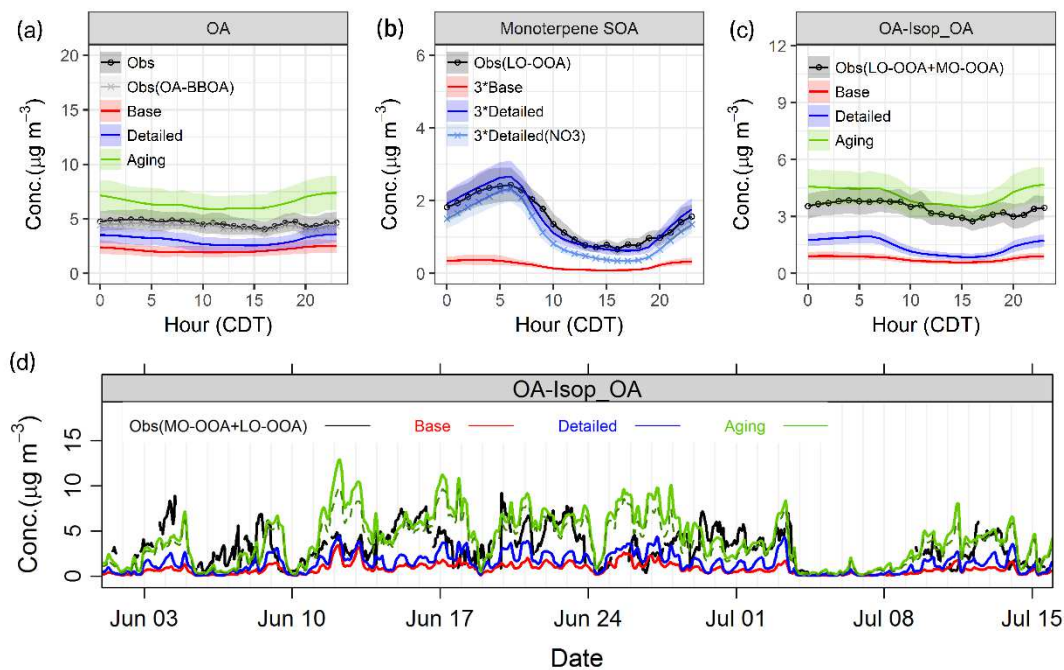
Fig. 4 Comparison of (a) observed and simulated organic aerosol (OA), (b) observed less-oxidized oxygenated OA (LO-OOA) and simulated monoterpene-formed secondary organic aerosol (SOA$_M$), (c) (d) observed sum of LO-OOA and more-oxidized oxygenated OA (MO-OOA) and simulated OA excluding isoprene-derived SOA (SOA$_I$) ((c) diurnal trend, (d) time series) at Centreville during the SOAS campaign.

(The base case is shown in red, with the detailed case shown in blue and the aging case shown in green. Additionally, observed OA subtracting biomass burning OA (BBOA) is shown in grey in (a), and SOA$_M$ formed from NO$_3$ chemistry is shown in light blue in (b). The shaded areas in (a), (b) and (c) reflect 95% Gaussian confidence intervals. The simulated OA, when only aging of initial SOA$_M$ was considered, is indicated with dashed line in (d).)
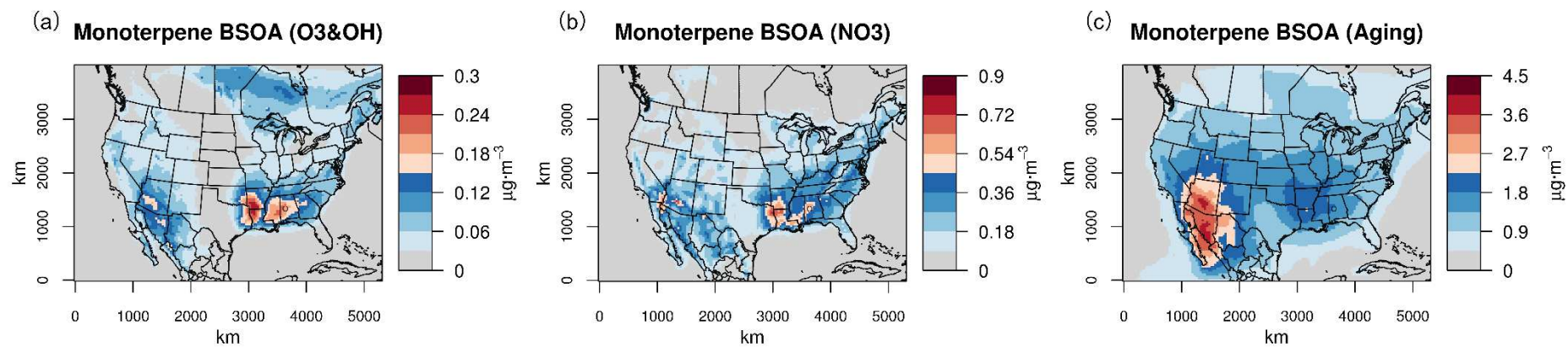
Fig. 5 Simulated monoterpene-formed SOA (SOA$_M$) via reactions with (a) dominant oxidants during the daytime i.e. OH and O$_3$, (b) dominant oxidant at night i.e. NO$_3$, (c) multigenerational oxidation during the SOAS campaign. The location of Centreville site is labeled as a circle.
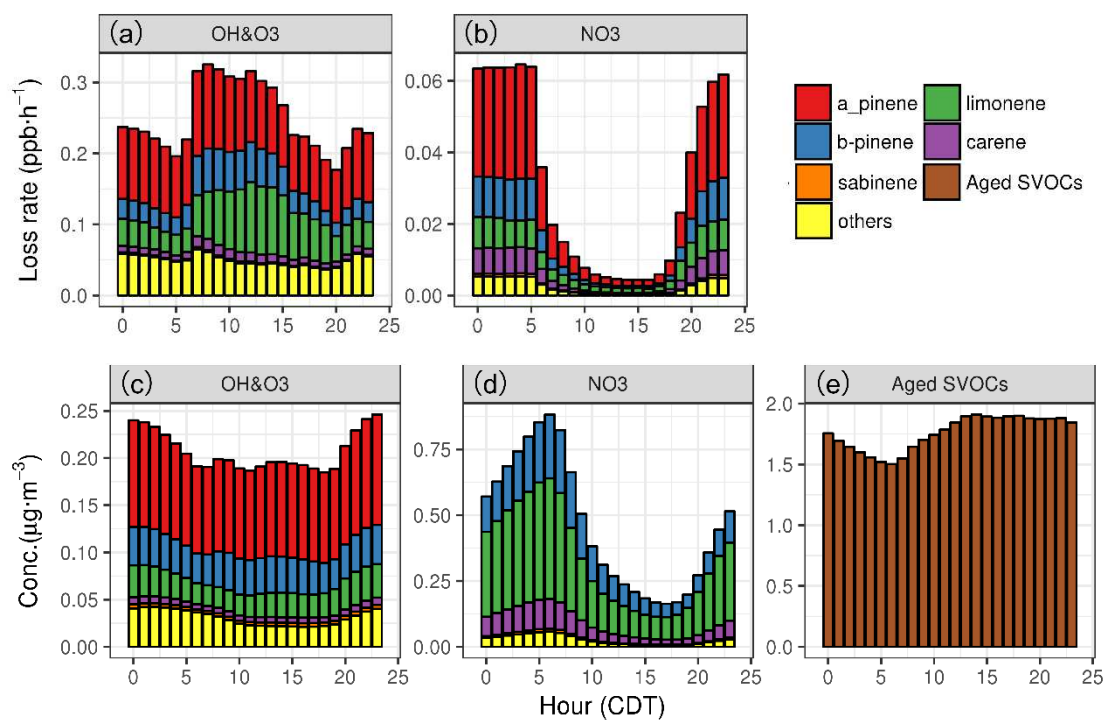
Fig. 6 Loss rate of monoterpenes to (a) dominant oxidants during the daytime i.e. OH and O_3, (b) dominant oxidant at night i.e. NO_3; monoterpene-formed SOA (SOA_M) contributed by (c) reactions with OH and O_3, (d) reactions with NO_3, (e) aged SVOCs at Centreville during the SOAS campaign.

Table 1 Evaluation of model performance on hourly oxidants (OH, O_3, NO_3), gas-phase organonitrates (ONs) and organic aerosol (OA) in the base, detailed, and aging case. Calculation of the metrics follows Yu et al. (2006).

Species	Case	FAC2[1]	MB[2]	NMB[3]	NME[4]	r[5]
OH	base	57.7	−0.0017	−7.3	52.3	0.63
	detailed	54.7	−0.0025	−10.7	52.7	0.64
	aging	54.9	-0.0027	-11.4	52.5	0.64
O_3	base	76.3	9.1	34.5	43.9	0.53
	detailed	78.2	8.8	33.5	42.6	0.58
	aging	78.5	8.7	32.9	42.2	0.59
NO_3	base	48.7	−0.012	−18.3	72.5	0.54
	detailed	43.3	0.033	48.3	100.5	0.51
	aging	43.4	0.032	46.8	99.7	0.51
Gaseous ONs	base	58.7	0.31	79.6	85.9	0.65
	detailed	55.5	0.34	90.0	95.6	0.65
	aging	55.6	0.33	88.8	94.4	0.65
OA^6	base	37.6	−2.0	−45.3	59.6	0.29
	detailed	52.4	−0.93	−21.4	52.6	0.32
	aging	57.1	2.9	66.5	84.4	0.36
$OA - isop\_OA^7$	base	15.3	−2.6	−74.5	76.2	0.30
	detailed	34.2	−1.8	−52.8	61.1	0.34
	aging	63.4	1.2	35.6	64.8	0.33

---

[1] FAC2, fraction of predictions within a factor or two

[2] MB, mean bias

[3] NMB, normalized mean bias

[4] NME, normalized mean error

[5] r, correlation coefficient

[6] compared to (OA – BBOA) in the observation

[7] compared to (MO-OOA + LO-OOA) in the observation

References

Yu, S., Eder, B., Dennis, R., Chu, S.H., Schwartz, S.E., 2006. New unbiased symmetric metrics for evaluation of air quality models. Atmospheric Science Letters 7, 26-34.